Mid-infrared emission and quantitative analysis of energy transfer processes in Er^{3+} doped oxyfluogermanate glasses

Muzhi Cai, Beier Zhou, Fengchao Wang, Ying Tian, Jiajia Zhou, Shiqing Xu,[a] and Junjie Zhang[a]
College of Materials Science and Engineering, China Jiliang University, Hangzhou 310018, People's Republic of China

(Received 24 April 2015; accepted 16 June 2015; published online 26 June 2015)

Oxyfluogermanate glasses with good thermal stability were prepared by melt-quenching method. The investigation of 2.7 μm fluorescence spectra and energy transfer mechanism was performed pumped by an 808 nm laser diode. The 2.7 μm radiative transition probability and emission cross section are 32.62 s^{-1} and 12.88 $\times 10^{-21}$ cm^2, respectively. The energy transfer parameters between $^4I_{11/2}$ and $^4I_{13/2}$ levels were calculated by Inokuti-Hirayama and Yokota-Tanimoto's model to further elucidate 2.7 μm fluorescent behaviors. It is found that the energy transfer mechanism among Er^{3+} is mainly dominated by dipole-dipole interactions. Results indicate that the prepared oxyfluogermanate glass is a promising candidate for mid-infrared laser applications. © *2015 AIP Publishing LLC*. [http://dx.doi.org/10.1063/1.4923064]

I. INTRODUCTION

The mid-infrared (MIR) wavelength range (2–5 μm), which covers important atmospheric windows, has drawn significant interests in the last decades because of the potential applications in civil and military fields.[1–3] To achieve efficient MIR emission, an appropriate host material and rare earth ions should be considered carefully. Rare earth ions for MIR emissions are mainly focused on Er^{3+}, Ho^{3+}, Dy^{3+}, and Pr^{3+} (Refs. 4–7) to date. Among them, Er^{3+} is deemed as an ideal candidate since it is capable of generating 2.7 μm luminescence via the $^4I_{11/2} \rightarrow {}^4I_{13/2}$ transition. Moreover, it is conveniently pumped by commercially available 808 nm or 980 nm laser diodes. On the other hand, the host has an important influence on the 2.7 μm emission. Last decades have witnessed the great development of mid-infrared materials such as crystal and glass.[6,8] Compared with crystal, glass has the merits of high solubility in rare earth ions and low cost. Up to now, many different kinds of glass have been investigated for mid-infrared applications including chalcogenide, fluoride, and heavy metal oxide glasses.[8–12] Although chalcogenide glass have quite low phonon energy and larger refractive index, it is difficult to draw into fiber due to its relatively low recrystallisation temperature which is close to the fiber drawing temperature.[13] Fluoride glass or fiber is a natural candidate as mid-infrared laser owing to its low phonon energy and superior infrared transmittance performance.[14] Based on this idea, in 2011, a maximum output power of 20.6 W at 2.825 μm was achieved from Er^{3+} doped fluoride fiber and the slope efficiency of the passively cooled laser was up to 35.4%.[15] In 2013, single-longitudinal-mode fiber laser operating at 2914 nm was demonstrated in Ho^{3+}/Pr^{3+} codoped ZBLAN fiber with a spectrometer-limited linewidth of <0.4 nm when pumped at 1150 nm.[16] In addition, Dy^{3+} doped ZBLAN fiber laser operating at 2.96 μm was also determined by ~1.3 μm Nd: YAG laser pumping.[17] Unfortunately, fluoride glass has the disadvantages of poor thermal stability, chemical durability, and mechanical strength.[14]

Heavy metal oxide glass has lower phonon energy than other oxide glasses (e.g., silicate and phosphate glasses) and better physicochemical stability than fluoride glass. Among heavy metal oxide glass, germanate glass is quite suitable as host material for mid-infrared laser contribution to the merits of excellent thermal stability, chemical durability, low maximum phonon energy, and high transparency in a wide wavelength region.[18] Due to a high concentration of hydroxyl groups might lead to a strong absorption band around 2.7 μm, which is harmful for corresponding mid-infrared emission, in recent years, BaF_2 and LiF additions are introduced to germanate glass to modify glass forming ability, and F^- ions in glass can minimize the contents of hydroxyl groups and phonon energy.[19]

In this work, oxyfluogermanate glasses were prepared and mid-infrared fluorescence properties were investigated pumped by an 808 nm laser diode. 975 nm and 1530 nm emission spectra and corresponding decay lifetimes were determined to elucidate 2.7 μm emission behaviors. Energy transfer parameters were also evaluated via Inokuti-Hirayama and Yokota-Tanimoto's models.

II. EXPERIMENTAL PROCEDURE

A. Sample preparation

Oxyfluogermanate glasses have the compositions of $87(GeO_2 + Ga_2O_3 + La_2O_3)$–$13(BaF_2 + LiF)$–$1Er_2O_3$ and $81(GeO_2 + Ga_2O_3 + La_2O_3)$–$19(BaF_2 + LiF)$–$1Er_2O_3$ (mol. %), denoted as FG-01 and FG-02, respectively. Powders of high-purity GeO_2, Ga_2O_3, BaF_2, La_2O_3, LiF, and Er_2O_3 were used as raw materials. Well-mixed 20 g batches of the sample were placed in a high-purity Al_2O_3 crucible and melted in a Si-Mo resistance furnace at 1400 °C for 40 min. Then, they

[a]Authors to whom correspondence should be addressed. Electronic addresses: jjzhang@cjlu.edu.cn and shiqingxu@cjlu.edu.cn

quenched on preheated stainless steel plate and annealed near the temperature of glass transition for 2 h before they were cooled to room temperature. The annealed samples were finally cut and optically polished to the size of 20 mm × 10 mm × 1.5 mm for the optical property measurements.

B. Performance measurements

The densities of samples were tested via the Archimedes principle using distilled water as the immersion medium with error of ±0.001 g/cm^3. Refractive indexes were measured by the prism minimum deviation method at the wavelength of 1053 nm with error limit of ±0.05%. Differential scanning calorimeter (DSC) curves were measured using NETZSCH DTA 404 PC at the heating rate of 10 K/min with error of ±5 °C. The characteristic temperatures (including temperatures of glass transformation, onset crystalline peak, and top crystalline peak) were determined by doing tangent at glass transformation point, near crystallization peak temperature, and top crystalline peak, respectively. Absorption spectra were obtained using a Perkin Elmer Lambda 900UV-VIS-NIR spectrophotometer in the range of 350–1640 nm with a resolution of 1 nm. Fluorescence spectra from 940 to 2800 nm were tested with a computer-controlled Triax 320 type spectrometer excited by an 808 nm laser diode. Excitation source with the same power was used to measure the fluorescence lifetimes of $^4I_{11/2}$ and $^4I_{13/2}$ level, which was recorded via HP546800B 100-MHz oscilloscope. The same experimental conditions for different samples were maintained so as to get comparable results. All the measurements were carried out at room temperature.

III. RESULTS AND DISCUSSION

A. Thermal stability analysis

Fig. 1 shows the DSC curves of oxyfluogermanate glasses. According to the thermal analysis, characteristic temperatures including temperatures of glass transition (T_g), onset crystallization peak (T_x), and top crystallization peak (T_p) are obtained as assigned in Fig. 1. Table I summarizes T_g, T_x, T_p, thermal stability parameters ΔT (T_x-T_g), and S in various glass hosts. Glass forming ability criterion, ΔT, has been frequently utilized to measure the glass stability and a large ΔT means strong inhibition of nucleation and crystallization. The ΔT of FG-01 and FG-02 glasses are calculated to be 158 °C and 130 °C, respectively. They are higher than that of fluorophosphate glass,[14] while comparable to those of bismuthate and germanate glasses.[8,12]

TABLE I. The glass transition temperature (T_g), onset crystallization temperature (T_x), top crystallization peak (T_p), thermal stability parameters ΔT and S in various glass hosts.

Glass samples	T_g (°C)	T_x (°C)	T_p (°C)	ΔT (°C)	S (K)	References
FG-01	608	766	796	158	5.38	This study
FG-02	599	729	786	130	8.50	
Germanate	618	747	769	129	4.59	12
Bismuthate	370	511	527	141	3.51	8
Fluorophosphate	462	549	565	87	1.89	10

The parameter S is more accurate to estimate the glass stability, which reflects the resistance to devitrification after the formation of the glass and can be defined by

$$S = \frac{\Delta T \times (T_p - T_x)}{T_g}, \quad (1)$$

where (T_p-T_x) is related to the rate of devitrification transformation of the glassy phases. On the other hand, the high value of ΔT delays the nucleation process. It is found that the S is 5.38 K and 8.50 K for FG-01 and FG-02, respectively. They are higher than those of bismuthate and fluorophosphate glass, while comparable to other germanate glass as shown in Table I.

Besides, a high T_g is beneficial to minimize the thermal damage when pumped by high power lasers.[12] It is found that the prepared samples possess a higher T_g compared with other glasses. Hence, oxyfluogermanate glasses with good thermal stability might be selected as laser materials.

B. Absorption spectra and Judd-Ofelt analysis

Fig. 2 indicates absorption spectra of oxyfluogermanate glasses at room temperature in the wavelength region of 350–1640 nm. Each absorption band corresponding to transitions from their ground state $^4I_{15/2}$ to higher levels $^4I_{13/2}$,

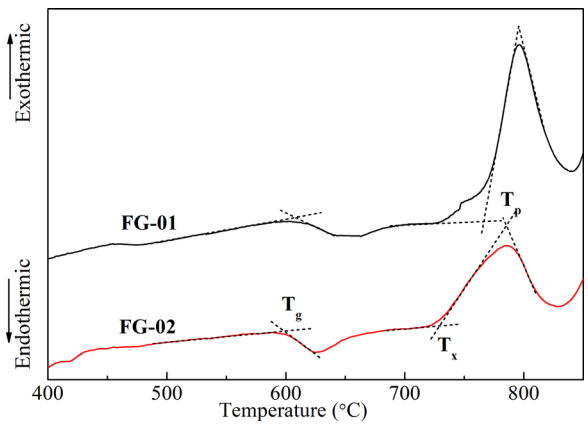

FIG. 1. DSC curves of oxyfluogermanate glasses.

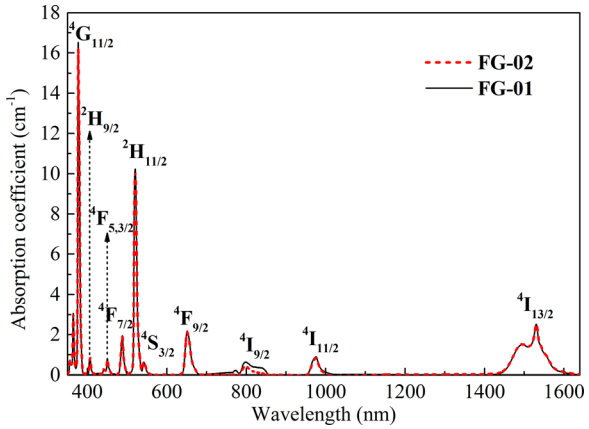

FIG. 2. Absorption spectra in Er^{3+} doped oxyfluogermanate glasses.

$^4I_{11/2}$, $^4I_{9/2}$, $^4F_{9/2}$, $^4S_{3/2}$, $^2H_{11/2}$, $^4F_{7/2}$, $^4F_{5/2}+{}^4F_{3/2}$, $^2H_{9/2}$, and $^4G_{11/2}$ is labeled. It is observed from Fig. 2 that the shape and peak positions of each transition are very similar in comparison to other Er^{3+} doped systems.[20,21] Some tiny divergences can be found originated from various ligand field strength of glass. Compared with other transitions, $^4I_{15/2} \rightarrow {}^4G_{11/2}$ and $^4I_{15/2} \rightarrow {}^2H_{11/2}$ transitions possess higher absorption coefficients, which are well-known hypersensitive transitions. They are sensitive to small changes of local environment around Er^{3+} ions.[22] In addition, the absorption band around 808 nm signifies that the prepared glasses can be pumped by commercially available 808 nm laser diode.

According to Judd-Ofelt (J-O) theory, intensity parameters $\Omega_{2,4,6}$ have been calculated from absorption spectra.[23,24] Table II lists J-O intensity parameters ($\Omega_{2,4,6}$) and root mean square deviation ($\delta_{r.m.s}$) of Er^{3+} in various glasses. It can be determined that $\delta_{r.m.s}$ in our samples are as low as 0.35×10^{-6} and 0.12×10^{-6}, respectively, indicating that the reliability and validity of the calculated J-O intensity parameters. Ω_λ are useful parameters for the investigation of the local structure and bonding in the vicinity of Er^{3+} ions. It has been reported that Ω_2 is sensitive to the environmental configuration symmetry of Er^{3+} ions and the amount of the covalent bonding.[25] It is observed that the Ω_2 of the prepared samples are lower than those of tellurite, bismuth-germanate, and other germanate glasses as shown in Table II. Results demonstrate that oxyfluogermanate glasses possess lower covalency of bonding and asymmetry of ligand environment surrounding Er^{3+} ions.

Based on J-O intensity parameters, the spontaneous radiative transition probability (A_{rad}) for Er^{3+}:$^4I_{11/2} \rightarrow {}^4I_{13/2}$ transition has been calculated and the A_{rad} is as high as $32.62\,s^{-1}$, which is larger than those of ZBLA ($19\,s^{-1}$) and fluoride glass ($29.04\,s^{-1}$),[9] while comparable to that of YAG ($33\,s^{-1}$).[9] High spontaneous transition probability is beneficial for high gain and more opportunity to achieve laser action.[29]

C. Fluorescence spectra and energy transfer mechanism

Fig. 2(a) indicates mid-infrared fluorescence spectra of FG-01 and FG-02 samples at the excitation of 808 nm laser diode. The emission peaks at 2.7 μm corresponding to the transition of $^4I_{11/2} \rightarrow {}^4I_{13/2}$ can be observed clearly. Moreover, the peak intensity of FG-02 is larger than that of FG-01. Fig. 2(b) shows the energy level diagram and energy transfer processes of Er^{3+} ions. It can be noted that the ions in ground state are populated to higher level $^4I_{9/2}$ at 808 nm pumping. Subsequently, populations in $^4I_{9/2}$ level relax to the lower $^4I_{11/2}$ level, quickly, owing to small energy gap between them. Afterwards, the ions in $^4I_{11/2}$ level decay radiatively to the ground state generating 975 nm emissions or radiatively relax to the $^4I_{13/2}$ level with 2.7 μm fluorescence. The ions in $^4I_{13/2}$ level decay radiatively to the ground state and 1.53 μm emissions take place.

Evidently, the population evolution between $^4I_{11/2}$ and $^4I_{13/2}$ levels has an influence on 2.7 μm fluorescence. Thus, it is necessary to investigate the emission spectra and lifetimes of $^4I_{11/2}$ and $^4I_{13/2}$ levels. Figs. 3(a) and 3(b) display the 975 nm and 1.53 μm fluorescence spectra, respectively. It is clear that the 975 nm emission due to $^4I_{11/2} \rightarrow {}^4I_{15/2}$ transition can be observed and the intensity of FG-02 sample is weaker than that of FG-01 sample. The strength of $^4I_{11/2} \rightarrow {}^4I_{13/2}$ transition can compete with that of $^4I_{11/2} \rightarrow {}^4I_{15/2}$ transition, so weak intensity of 975 nm emission is favorable for 2.7 μm emission. It is also observed from Fig. 3(b) that 1.53 μm fluorescence intensity of FG-02 sample is weaker than that of FG-01 sample. Weak 1.53 μm emission may be due to the reduced populations of $^4I_{13/2}$ level, which is beneficial for population inversion between $^4I_{11/2}$ and $^4I_{13/2}$ level. Hence, 2.7 μm emission intensity of FG-02 sample is higher than that of FG-01 sample.

975 nm and 1.53 μm fluorescent lifetimes are important parameters to estimate population evolution of $^4I_{11/2}$ and $^4I_{13/2}$ levels. According to the measured decay data, energy transfer parameter can be determined to analyze quantitatively energy transfer processes such as energy transfer upconversion (ETU1 and ETU2) as shown in Fig. 4(b).

Inokuti-Hirayama's (I-H) model can be utilized to evaluate the energy transfer processes among Er^{3+} ions, which is expressed as

$$\frac{I(t)}{I(0)} = \exp\left(-\frac{t}{\tau_0} - Q\left(\frac{t}{\tau_0}\right)^{3/S}\right), \tag{2}$$

where S is 6, 8, or 10 depending on whether the dominant mechanism of interaction is dipole-dipole, dipole-quadrupole, or quadrupole-quadrupole, respectively. τ_0 is the intrinsic lifetime. The energy transfer parameter (Q) is defined as

$$Q = \frac{4\pi}{3}\Gamma\left(1 - \frac{3}{S}\right)N_{Er}R_c^3, \tag{3}$$

where $\Gamma(1–3/S)$ is equal to 1.77 for dipole-dipole interactions (S = 6), 1.43 for dipole-quadrupole interactions (S = 8), and 1.3 in the case of quadrupole-quadrupole interactions (S = 10). N_{Er} is the concentration of Er^{3+} ions (in ions cm^{-3})

TABLE II. The J-O intensity parameters ($\times 10^{-20} cm^2$) and root mean square deviation ($\times 10^{-6}$) of Er^{3+} in various glasses.

Glass samples	Ω_2	Ω_4	Ω_6	$\delta_{r.m.s}$	References
FG-01	4.71 ± 0.01	2.04 ± 0.04	0.82 ± 0.03	0.35	Present work
FG-02	4.67 ± 0.02	1.84 ± 0.03	0.92 ± 0.02	0.12	
Bismuth-germanate	5.57	2.49	4.53	…	26
Germanate	6.59	2.77	1.90	0.47	27
Tellurite	8.47	1.72	1.01	…	28

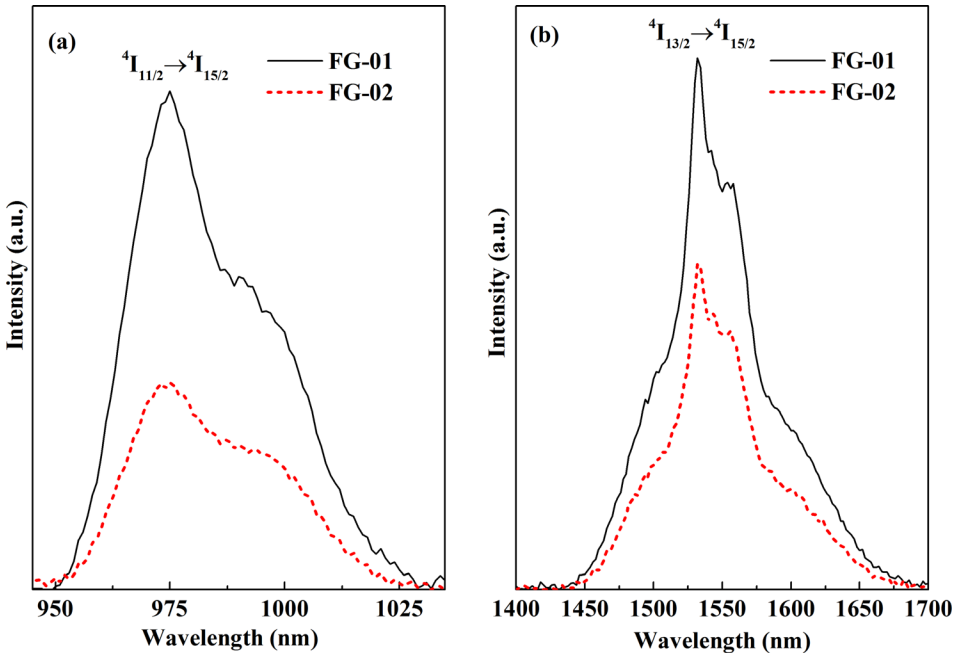

FIG. 3. (a) 975 nm and (b) 1.53 μm emission spectra in Er^{3+} doped oxyfluogermanate glasses.

and R_c is the critical transfer distance defined as the donor-acceptor separation for which the energy transfer rate is equal to the rate of intrinsic decay of the donors. Then, the energy transfer rate (C_{DA}) can be given by

$$C_{DA} = \frac{9Q^2}{8\pi N_{Er}^2 \Gamma(1-3/S)\tau_0}. \quad (4)$$

Figs. 5(a) and 5(b) show fitting results of decay curves for 975 nm and 1.53 μm emissions via I-H model. Relevant parameters were obtained as listed in Table III. The fitted results are reliable due to high values of Adj. R-Square. It is found that the C_{DA} of FG-02 sample is very similar to that of FG-01 sample for the $^4I_{11/2}$ level, whereas the C_{DA} of FG-02 sample is larger than that of FG-01 sample for the $^4I_{13/2}$ level. It is indicated that FG-02 sample is more beneficial to the population inversion between $^4I_{11/2}$ and $^4I_{13/2}$ level due to its faster energy transfer rate of $^4I_{13/2}$ level compared with FG-01 sample. Thus, the 2.7 μm emission of FG-02 sample is stronger than that of FG-01 sample.

Furthermore, the S values are determined to be 5.795–6.575, which are close to 6, indicating the dipole-dipole interactions among Er^{3+} ions. The deviation from 6 could be attributed to the migration effect (or diffusion effect) among Er^{3+} ions.[30] In this case, Yokota-Tanimoto's model is used to estimate both energy transfer and diffusion processes by assuming that dipole-dipole interaction is a dominant mechanism.[31] The expression is as follows:

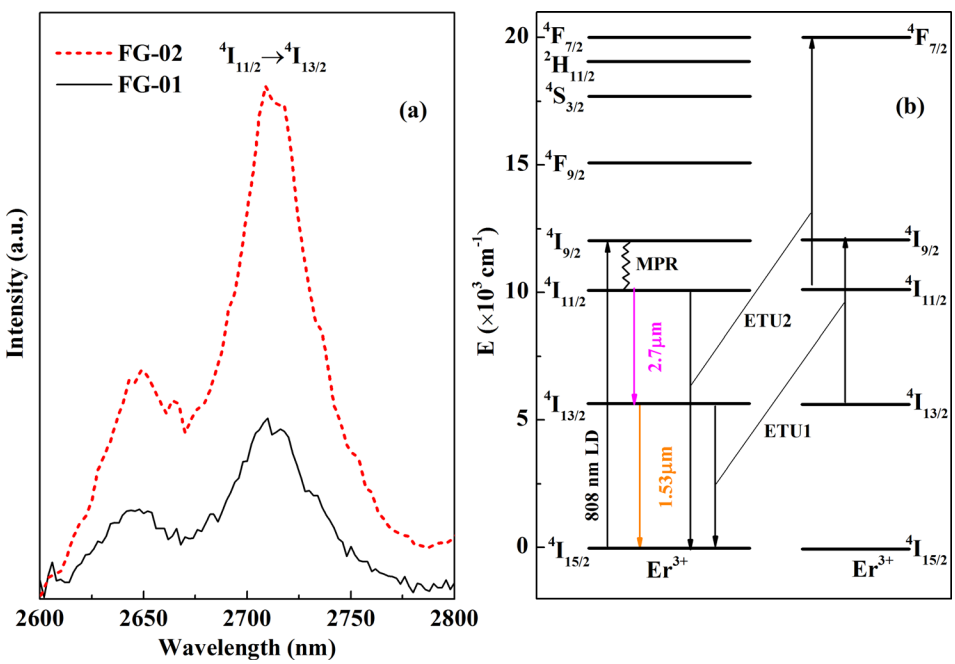

FIG. 4. (a) 2.7 μm fluorescence spectra and (b) energy level diagram of Er^{3+} in oxyfluogermanate glasses.

$$I(t) = I_0 \exp\left\{-\frac{t}{\tau_0} - \pi^{\frac{1}{2}} A \left(\frac{t}{\tau_0}\right)^{\frac{1}{2}} \left[\frac{1 + 10.87B\left(\frac{t}{\tau_0}\right)^{\frac{2}{3}} + 15.5B^2\left(\frac{t}{\tau_0}\right)^{\frac{4}{3}}}{1 + 8.743B\left(\frac{t}{\tau_0}\right)^{\frac{2}{3}}}\right]^{0.75}\right\}, \quad (5)$$

where $A = \frac{4}{3}\pi N_A C_{DA}^{\frac{1}{2}}$, $B = D\, C_{DA}^{-\frac{1}{3}}$. N_A is the concentration of Er^{3+} ions and C_{DA} is the energy transfer microparameter of Er^{3+} ions. The fitted results of decay curves are shown in Figs. 5(c) and 5(d). The fitted parameters are also summarized in Table III. Good match between measured date and fitted curves signifies the validity and reliability of results. In Table III, one can find small changes of C_{DA} values for $^4I_{11/2}$ level in prepared samples. However, the C_{DA} of $^4I_{13/2}$ level in FG-02 sample is much larger than that of FG-01 sample. High energy transfer rate of $^4I_{13/2}$ level is helpful to minimize the ions of this level and achieve population inversion between $^4I_{11/2}$ and $^4I_{13/2}$ levels. Results suggest that FG-02 sample is more beneficial for 2.7 μm emissions.

D. Cross sections and gain spectra

To further understand 2.7 μm emission properties, absorption and emission cross sections have been calculated and discussed. The absorption and emission cross sections can be obtained by Füchtbauer-Ladenburg equation[32] and McCumber theory[33]

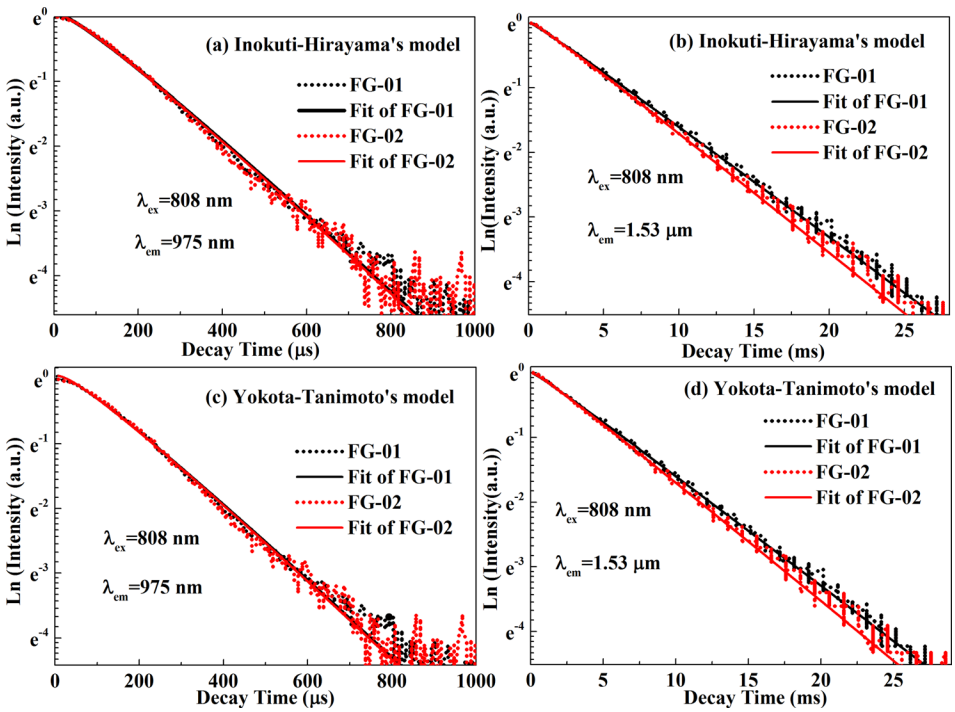

FIG. 5. Decay data and fitted curves of (a) 975 nm and (b) 1.53 μm via Inokuti-Hirayama's model; (c) 975 nm and (d) 1.53 μm via Yokota-Tanimoto's model.

TABLE III. The determined interaction factor S, energy transfer parameter Q and C_{DA} fitted by Inokuti-Hirayama's model as well as the parameters A, B, and C_{DA} fitted by Yokota-Tanimoto's model for 975 nm and 1.53 μm emissions in Er^{3+} doped oxyfluogermanate glasses.

	Inokuti-Hirayama's model			Yokota-Tanimoto's model		
Sample	Parameter	975 nm	1.53 μm	Parameter	975 nm	1.53 μm
FG-01	S	5.795 (±0.055)	6.575 (±0.206)	A	0.253 (±0.002)	0.071 (±0.002)
	Q	0.443 (±0.002)	0.125 (±0.002)	B	0.005 (±0.004)	0.007 (±0.017)
	C_{DA} (cm^6/s)	1.52×10^{-39}	3.32×10^{-42}	C_{DA} (cm^6/s)	2.09×10^{-44}	1.64×10^{-45}
	Adj. R-Square	0.998	0.999	Adj. R-Square	0.998	0.999
FG-02	S	5.796 (0.064)	6.485 (±0.117)	A	0.254 (±0.002)	0.093 (±0.002)
	Q	0.444 (±0.002)	0.165 (±0.001)	B	0.0074 (±0.005)	0.009 (±0.010)
	C_{DA} (cm^6/s)	1.54×10^{-39}	3.65×10^{-42}	C_{DA} (cm^6/s)	2.11×10^{-44}	2.83×10^{-45}
	Adj. R-Square	0.997	0.999	Adj. R-Square	0.997	0.999

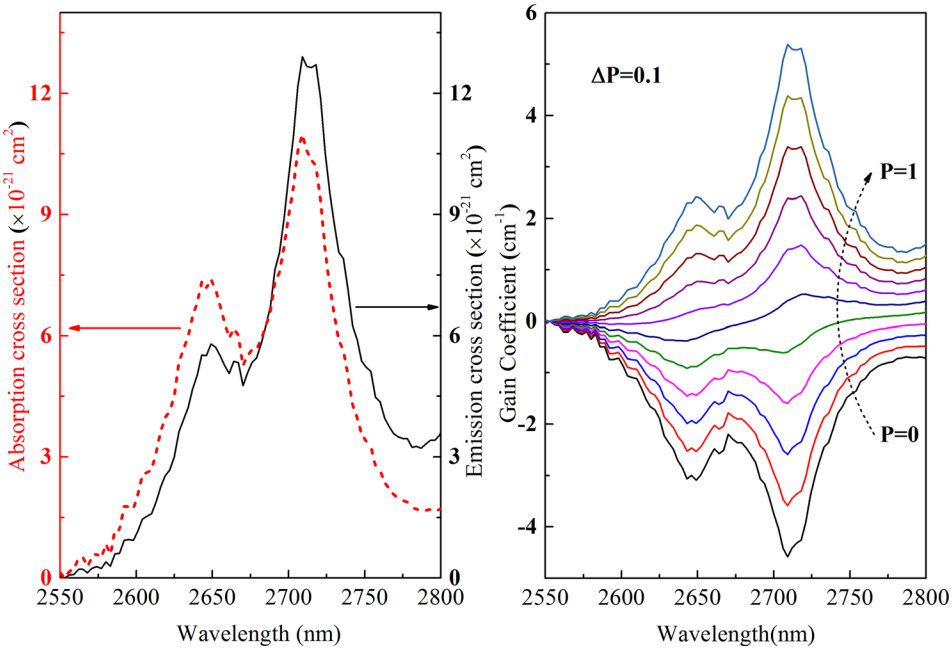

FIG. 6. (a) Calculated absorption and emission cross sections (b) gain spectra for $^4I_{11/2} \rightarrow {}^4I_{13/2}$ transition in Er^{3+} doped oxyfluogermanate glass.

$$\sigma_{em}(\lambda) = \frac{\lambda^4 A_{rad}}{8\pi c n^2} \times \frac{\lambda I(\lambda)}{\int \lambda I(\lambda) d\lambda}, \tag{6}$$

$$\sigma_{em}(\lambda) = \sigma_{abs}(\lambda)(Z_l/Z_u)\exp[(\varepsilon - h\nu)/kT], \tag{7}$$

where λ is the wavelength, A_{rad} is the spontaneous radiative transition probability, $I(\lambda)$ is the fluorescence spectra intensity, n and c represent the refractive index and the speed of light, Z_l and Z_u are partition functions of the lower and upper manifolds, respectively. ε is the net free energy demanded to excite one Er^{3+} from the $^4I_{13/2}$ to $^4I_{11/2}$ state at the temperature of T.

Fig. 6(a) displays the absorption and emission cross sections corresponding to Er^{3+}: $^4I_{11/2} \rightarrow {}^4I_{13/2}$ transition in Er^{3+} doped oxyfluogermanate glass. It is shown that the peak absorption (σ^p_{abs}) and emission cross sections (σ^p_{em}) are 10.98×10^{-21} cm^2 and 12.90×10^{-21} cm^2, respectively. The prepared glass possesses much higher σ^p_{em} compared with ZBLAY glass (9.16×10^{-21} cm^2)[9] and ZBLAN glass (5.7×10^{-21} cm^2).[34] Higher emission cross section has larger opportunity to achieve laser action.[22] Therefore, the prepared oxyfluogermanate glass would be an appropriate host to achieve efficient 2.7 μm laser using an 808 nm laser diode.

Gain coefficient is another characteristic parameter to evaluate 2.7 μm emission properties quantitatively. The wavelength dependent gain coefficient is calculated in detail as a function of population inversion for the upper laser level on the basis of the σ_{abs} and σ_{em}. The room temperature gain coefficient (G(λ,P)) can be simply denoted as

$$G(\lambda, P) = N[P\sigma_{em}(\lambda) - (1-P)\sigma_{abs}(\lambda)], \tag{8}$$

where N is the total concentration of Er^{3+} and P is the population inversion given by the ratio between the population of Er^{3+}: $^4I_{11/2}$ level and the total Er^{3+} concentration.

The calculated gain spectra of oxyfluogermanate glass are shown in Fig. 6(b). It can be observed that the gain coefficient is as high as 5.38 cm^{-1}, which is significantly larger than those of fluorotellurite (2.16 cm^{-1})[35] and ZBLAN glasses (0.6 cm^{-1}).[34] Furthermore, the positive gain can be obtained in the range of 2685–2800 nm when $P > 0.4$, similar to the case of ZBLAN.[14]

In addition, based on the theory derived by Giles and Desurvire for modeling fiber amplifiers,[36] the gain per unit length g at frequency ν and position z can be expressed as[37]

$$g_v(z) = N_0\Gamma_v\{\sigma_{ev}n_e(z) - \sigma_{av}(1 - n_e(z))\}, \tag{9}$$

where N_0 is the total rare-earth-ion and Γ_ν is the normalized spatial overlap between the propagating mode and the rare-earth concentration profile. σ_{av} and σ_{ev} are the wavelength dependent absorption and emission cross-sections of Er^{3+} ions, respectively. n_e is the normalized excited-state population density. Equation (9) indicates that the maximum gain per unit length g_v is mainly determined by the emission and absorption cross-sections as well as the population inversion of the active ions. Considering a general case with a spatial overlap Γ_ν of 100% and normalized excited-state population density n_e of 80%, the maximum gain per unit length at 2.7 μm could be as high as 3.3 dB/cm in a 1 mol. % Er^{3+}-doped FG-02. These indicate that the prepared glass has high gain and low pumping threshold for the 2.7 μm laser action.

IV. CONCLUSIONS

Oxyfluogermanate glasses with good thermal properties have been prepared. Furthermore, 2.7 μm fluorescence properties and energy transfer mechanism have been investigated under the excitation of an 808 nm laser diode. The prepared sample possesses high spontaneous radiative transition probability (32.64 s^{-1}), large emission cross section (12.90×10^{-21} cm^2), and good gain performance for Er^{3+}: $^4I_{11/2} \rightarrow {}^4I_{13/2}$ transition. The decay data of $^4I_{11/2}$ and $^4I_{13/2}$ levels have been measured and their energy transfer parameters have been determined by fitting decay curves to Inokuti-

Hirayama and Yokota-Tanimoto's models, respectively. It is found that dipole-dipole interaction is dominant mechanism among Er^{3+} ions via Inokuti-Hirayama's model. It is indicated that the oxyfluogermanate glass is an attractive laser material for mid-infrared applications.

ACKNOWLEDGMENTS

This research was financially supported by the Chinese National Natural Science Foundation (Nos. 51172252, 51372235, 61308090, and 51272243) and Zhejiang Provincial Natural Science Foundation of China (Nos. LR14E020003, LY13F050003, and LY14E020007).

[1]S. D. Jackson, Appl. Phys. Lett. **83**, 1316 (2003).
[2]W. Tianshu, W. Yizhen, H. Kai, Z. Peng, J. Qingsong, and J. Huilin, Microwave Opt. Technol. Lett. **56**, 848 (2014).
[3]G. S. Henderson and M. E. Fleet, J. Non-Cryst. Solids **134**, 259 (1991).
[4]F. Tong, W. P. Risk, R. M. MacFarlane, and W. Lenth, *Electronics Letters* (Institution of Engineering and Technology, 1989), Vol. 25, p. 1389.
[5]L. Gomes and S. D. Jackson, J. Opt. Soc. Am. B **30**, 1410 (2013).
[6]X. Zhuang, H. Xia, H. Hu, J. Hu, P. Wang, J. Peng, Y. Zhang, H. Jiang, and B. Chen, Mater. Sci. Eng., B **178**, 326 (2013).
[7]A. Sennaroglu, Y. H. Tsang, A. E. El-Taher, T. A. King, K.-P. Chang, and S. D. Jackson, Proc. of SPIE **6190**, 61900J (2006).
[8]G. Zhao, Y. Tian, H. Fan, J. Zhang, and L. Hu, Chin Opt. Lett. **10**, 091601 (2012).
[9]Y. Tian, R. Xu, L. Hu, and J. Zhang, Opt. Mater. **34**, 308 (2011).
[10]M. Liao, H. Sun, L. Wen, Y. Fang, and L. Hu, Mater. Chem. Phys. **98**, 154 (2006).
[11]Y. Guo, Y. Ma, F. Huang, Y. Peng, L. Zhang, and J. Zhang, Spectrochim. Acta, Part A **111**, 150 (2013).
[12]R. Xu, Y. Tian, L. Hu, and J. Zhang, Opt. Lett. **36**, 1173 (2011).
[13]D. J. Coleman, S. D. Jackson, P. S. Golding, T. A. King, S. H. Park, Y. B. Shin, and J. Heo, in *Heavy Metal Oxide and Chalcogenide Glasses as New Hosts for Er^{3+} and Er^{3+}/Pr^{3+}Mid-IR Fiber Lasers* (Optical Society of America, Davos, Switzerland, 2000), p. MB10.
[14]F. Huang, Y. Ma, W. Li, X. Liu, L. Hu, and D. Chen, Sci. Rep. **4**, 3607 (2014).
[15]D. Faucher, M. Bernier, G. Androz, N. Caron, and R. Vallée, Opt. Lett. **36**, 1104 (2011).
[16]D. D. Hudson, R. J. Williams, M. J. Withford, and S. D. Jackson, Opt. Lett. **38**, 2388 (2013).
[17]Y. H. Tsang, A. E. El-Taher, T. A. King, and S. D. Jackson, Opt. Express **14**, 678 (2006).
[18]R. Xu, Y. Tian, L. Hu, and J. Zhang, J. Appl. Phys. **111**, 033524 (2012).
[19]G. Cao, F. Lin, H. Hu, and F. Gan, J. Non-Cryst. Solids **326–327**, 170 (2003).
[20]X. Li, X. Liu, L. Zhang, L. Hu, and J. Zhang, Chin Opt. Lett. **11**, 121601 (2013).
[21]J. Hu, H. Xia, H. Hu, X. Zhuang, Y. Zhang, H. Jiang, and B. Chen, Mater. Res. Bull. **48**, 2604 (2013).
[22]Y. Tian, R. Xu, L. Hu, and J. Zhang, J. Quantum Spectrosc. Radiat. Transfer **113**, 87 (2012).
[23]B. Judd, Phys. Rev. **127**, 750 (1962).
[24]G. S. Ofelt, J. Chem. Phys. **37**, 511 (1962).
[25]Y. V. Orlovskii, T. T. Basiev, K. K. Pukhov, O. K. Alimov, N. A. Glushkov, and V. A. Konyushkin, Opt. Mater. **32**, 599 (2010).
[26]X. Li, Q. Nie, S. Dai, T. Xu, L. Lu, and X. Zhang, J. Alloys Compd. **454**, 510 (2008).
[27]J. Fan, Y. Fan, Y. Yang, D. Chen, L. Calveza, X. Zhang, and L. Zhang, J. Non-Cryst. Solids **357**, 2431 (2011).
[28]H. Lin, D. Chen, Y. Yu, A. Yang, and Y. Wang, Opt. Lett. **36**, 1815 (2011).
[29]J. Heo, Y. B. Shin, and J. N. Jang, Appl. Opt. **34**, 4284 (1995).
[30]K.-S. Sohn, Y. Y. Choi, and H. D. Park, J. Electrochem. Soc. **147**, 1988 (2000).
[31]V. Moizan, V. Nazabal, J. Troles, P. Houizot, J.-L. Adam, J.-L. Doualan, R. Moncorge, F. Smektala, G. Gadret, S. Pitois, and G. Canat, Opt. Mater. **31**, 39 (2008).
[32]S. A. Payne, L. Chase, L. K. Smith, W. L. Kway, and W. F. Krupke, IEEE J. Quantum Electron. **28**, 2619 (1992).
[33]D. McCumber, Phys. Rev. **136**, A954 (1964).
[34]B. Wang, L. Cheng, H. Zhong, J. Sun, Y. Tian, X. Zhang, and B. Chen, Opt. Mater. **31**, 1658 (2009).
[35]Y. Ma, Y. Guo, F. Huang, Y. Peng, L. Hu, and J. Zhang, J. Non-Cryst. Solids **369**, 23 (2013).
[36]C. R. Giles and E. Desurvire, J. Lightwave Technol. **9**(2), 271–283 (1991).
[37]J. L. Wagener, D. G. Falquier, M. J. F. Digonnet, and H. J. Shaw, J. Lightwave Technol. **16**(2), 200–206 (1998).